Atmospheric
Chemistry
and Physics

Open Access

EGU

Supplement of

Molecular composition and volatility of multi-generation products formed from isoprene oxidation by nitrate radical

Rongrong Wu et al.

Correspondence to: Thomas F. Mentel (t.mentel@fz-juelich.de)

Table S1: Possible permutation scheme for dimers formed through $RO_2 + R'O_2$ reactions. Molecular formulas presented in dark colors (colored by isomers) are compounds detected by CIMS in this study, while those in light grey were not.

$C_5H_8NO_x$ / $C_5H_8NO_x$	O_5	O_6	O_7	O_8	O_9
O_5	$C_{10}H_{16}N_2O_8$				
O_6	$C_{10}H_{16}N_2O_9$	$C_{10}H_{16}N_2O_{10}$			
O_7	$C_{10}H_{16}N_2O_{10}$	$C_{10}H_{16}N_2O_{11}$	$C_{10}H_{16}N_2O_{12}$		
O_8	$C_{10}H_{16}N_2O_{11}$	$C_{10}H_{16}N_2O_{12}$	$C_{10}H_{16}N_2O_{13}$		
O_9	$C_{10}H_{16}N_2O_{12}$	$C_{10}H_{16}N_2O_{13}$	$C_{10}H_{16}N_2O_{14}$		
O_{10}	$C_{10}H_{16}N_2O_{13}$	$C_{10}H_{16}N_2O_{14}$	$C_{10}H_{16}N_2O_{15}$		
O_{11}	$C_{10}H_{16}N_2O_{14}$	$C_{10}H_{16}N_2O_{15}$	$C_{10}H_{16}N_2O_{16}$		
O_{12}	$C_{10}H_{16}N_2O_{15}$	$C_{10}H_{16}N_2O_{16}$	$C_{10}H_{16}N_2O_{17}$		

$C_5H_8NO_x$ / $C_5H_9N_2O_y$	O_5	O_6	O_7	O_8	O_9
O_9	$C_{10}H_{17}N_3O_{12}$	$C_{10}H_{17}N_3O_{13}$	$C_{10}H_{17}N_3O_{14}$	$C_{10}H_{17}N_3O_{15}$	$C_{10}H_{17}N_3O_{16}$
O_{10}	$C_{10}H_{17}N_3O_{13}$	$C_{10}H_{17}N_3O_{14}$	$C_{10}H_{17}N_3O_{15}$	$C_{10}H_{17}N_3O_{16}$	$C_{10}H_{17}N_3O_{17}$
O_{11}	$C_{10}H_{17}N_3O_{14}$	$C_{10}H_{17}N_3O_{15}$	$C_{10}H_{17}N_3O_{16}$	$C_{10}H_{17}N_3O_{17}$	$C_{10}H_{17}N_3O_{18}$
O_{12}	$C_{10}H_{17}N_3O_{15}$	$C_{10}H_{17}N_3O_{16}$	$C_{10}H_{17}N_3O_{17}$	$C_{10}H_{17}N_3O_{18}$	$C_{10}H_{17}N_3O_{19}$
O_{13}	$C_{10}H_{17}N_3O_{16}$	$C_{10}H_{17}N_3O_{17}$	$C_{10}H_{17}N_3O_{18}$	$C_{10}H_{17}N_3O_{19}$	$C_{10}H_{17}N_3O_{20}$
O_{14}	$C_{10}H_{17}N_3O_{17}$	$C_{10}H_{17}N_3O_{18}$	$C_{10}H_{17}N_3O_{19}$	$C_{10}H_{17}N_3O_{20}$	$C_{10}H_{17}N_3O_{21}$
O_{15}	$C_{10}H_{17}N_3O_{18}$	$C_{10}H_{17}N_3O_{19}$	$C_{10}H_{17}N_3O_{20}$	$C_{10}H_{17}N_3O_{21}$	$C_{10}H_{17}N_3O_{22}$
O_{16}	$C_{10}H_{17}N_3O_{19}$	$C_{10}H_{17}N_3O_{20}$	$C_{10}H_{17}N_3O_{21}$	$C_{10}H_{17}N_3O_{22}$	$C_{10}H_{17}N_3O_{23}$
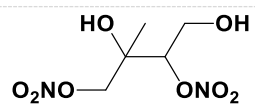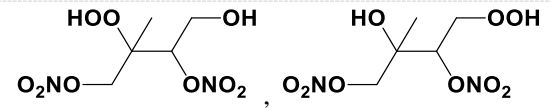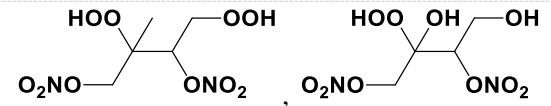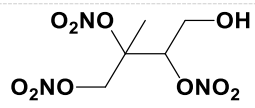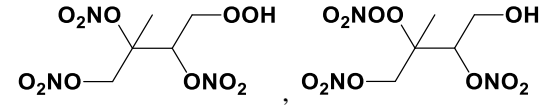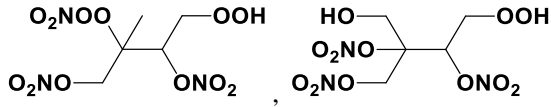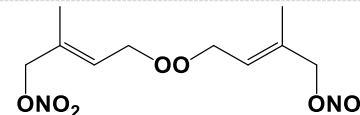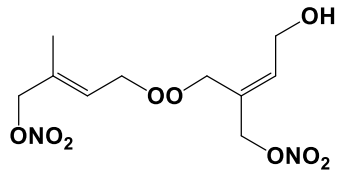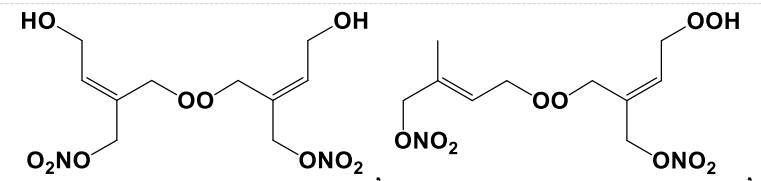
$C_5H_9N_2O_y$ / $C_5H_9N_2O_y$	O_9	O_{10}	O_{11}	O_{12}	O_{13}
O_9	$C_{10}H_{18}N_4O_{16}$				
O_{10}	$C_{10}H_{18}N_4O_{17}$				
O_{11}	$C_{10}H_{18}N_4O_{18}$				
O_{12}	$C_{10}H_{18}N_4O_{19}$				
O_{13}	$C_{10}H_{18}N_4O_{20}$				
O_{14}	$C_{10}H_{18}N_4O_{21}$				
O_{15}	$C_{10}H_{18}N_4O_{22}$				
O_{16}	$C_{10}H_{18}N_4O_{23}$				

Table S2: Ions observed in the gas phase by CIMS and proposed possible products from isoprene oxidation by NO₃

No.	Molecular formula	Molecular weight	Observed m/z (-)	Proposed structure
1	$C_4H_7NO_5$	149	228, 230	
2	$C_5H_7NO_4$	145	224, 226	
3	$C_5H_7NO_5$	161	240, 242	
4	$C_5H_7NO_6$	177	256, 258	
5	$C_5H_7NO_7$	193	272, 274	
6	$C_5H_9NO_4$	147	226, 228	
7	$C_5H_9NO_5$	163	242, 244	
8	$C_5H_9NO_6$	179	258, 260	

3

9	$C_5H_9NO_7$	195	274, 276	
10	$C_4H_6N_2O_7$	194	273, 275	
11	$C_5H_6N_2O_8$	222	301, 303	
12	$C_5H_8N_2O_7$	208	287, 289	
13	$C_5H_8N_2O_8$	224	303, 305	
14	$C_5H_8N_2O_9$	240	319, 321	
15	$C_5H_8N_2O_{10}$	256	335, 337	

No.	Formula			Structure
16	$C_5H_{10}N_2O_8$	226	305, 307	
17	$C_5H_{10}N_2O_9$	242	321, 323	
18	$C_5H_{10}N_2O_{10}$	258	337, 339	
19	$C_5H_9N_3O_{10}$	271	350, 352	
20	$C_5H_9N_3O_{11}$	287	366, 368	
21	$C_5H_9N_3O_{12}$	303	382, 384	
22	$C_{10}H_{16}N_2O_8$	292	371, 373	
23	$C_{10}H_{16}N_2O_9$	308	387, 389	
24	$C_{10}H_{16}N_2O_{10}$	324	403, 405	

5

| 25 | $C_{10}H_{16}N_2O_{11}$ | 340 | 419, 421 |
| 26 | $C_{10}H_{16}N_2O_{12}$ | 356 | 435, 437 |

| 27 | $C_{10}H_{16}N_2O_{13}$ | 372 | 451, 453 | |

| 28 | $C_{10}H_{17}N_3O_{12}$ | 371 | 450, 452 | |

| 29 | $C_{10}H_{17}N_3O_{13}$ | 387 | 466, 468 | |

| 30 | $C_{10}H_{17}N_3O_{14}$ | 403 | 482, 484 | |
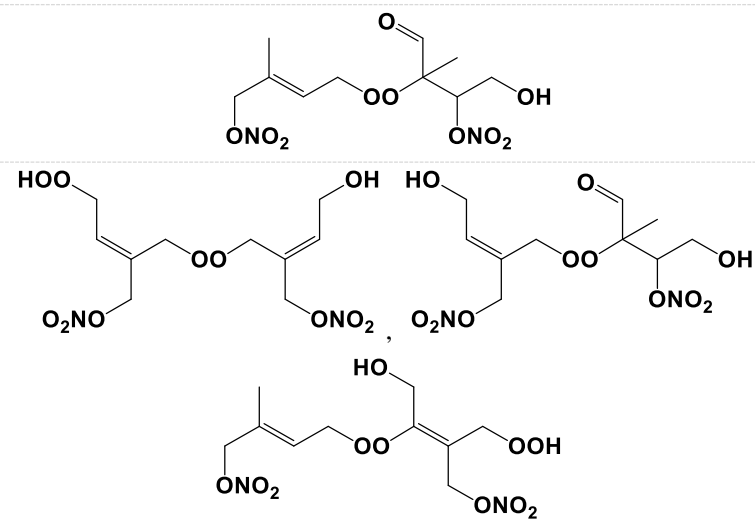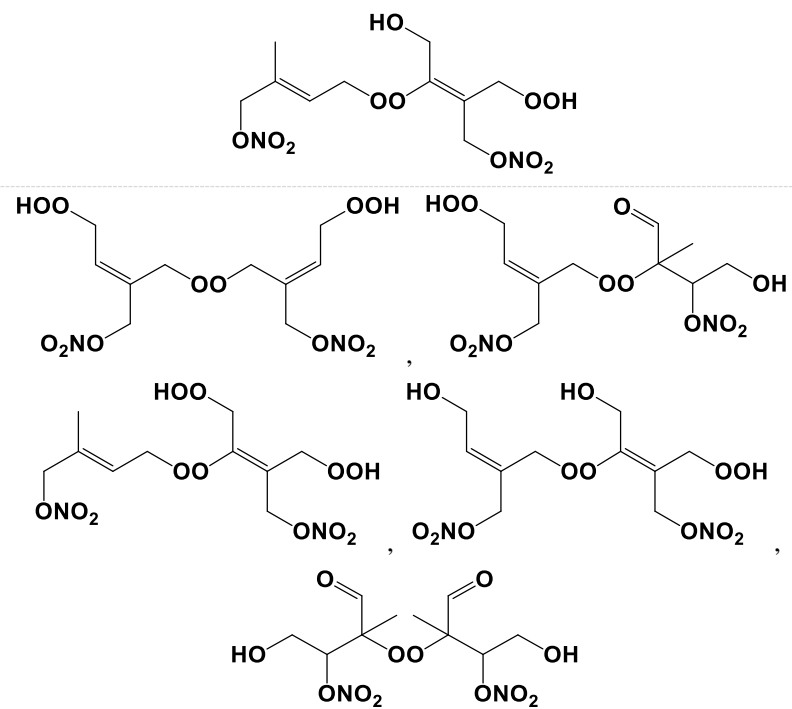
				,
31	$C_{10}H_{17}N_3O_{15}$	419	498, 500	, ,
32	$C_{10}H_{17}N_3O_{16}$	435	514, 516	, ,

8
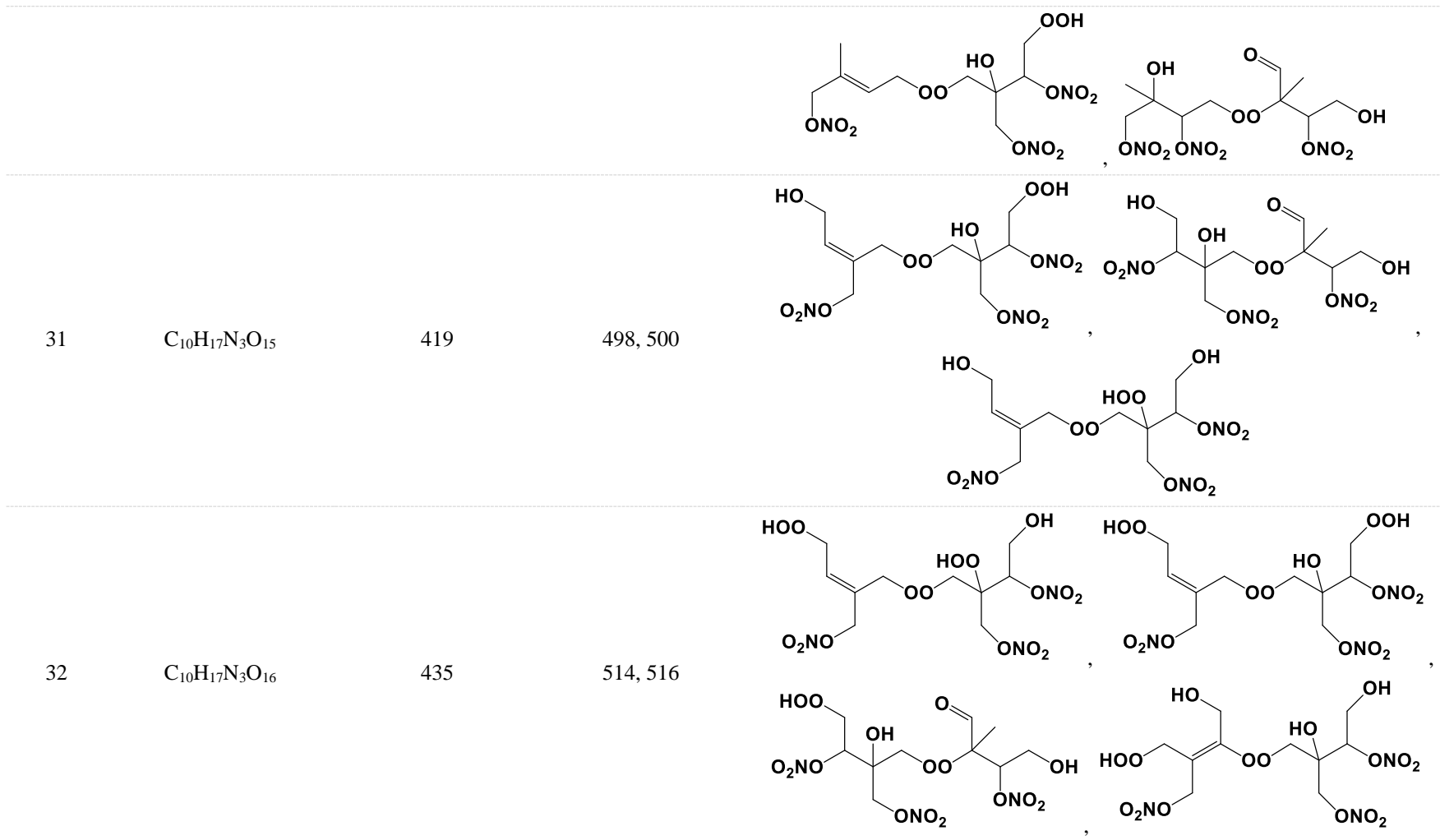
Table S3 lists the wall loss rates of dimers that used for wall-loss correction. Assuming that the dimers undergo irreversible gas-wall partitioning, then the overall wall loss rate of an organic species i ($k_{w,i}$) can be written as Eq. (S1) (Zhang et al., 2015).

$$k_{w,i}=\left(\frac{A}{V}\right)\left(\frac{\alpha_{w,i}\bar{v}_i/4}{\pi\alpha_{w,i}\bar{v}_i/8\left(D_iK_e\right)^{1/2}+1}\right) \tag{S1}$$

where A/V is the surface to volume ratio of the SAPHIR chamber, $\alpha_{w,i}$ is the mass accommodation coefficient of species i onto the chamber wall, $\bar{v}_i$ is the mean thermal speed of species i, D_i is the molecular diffusivity, and K_e is the coefficient of eddy diffusion. D_i varies with molecular weight (MW) and is equal to $D_{CO_2}\times\left(MW_{CO_2}/MW_i\right)$ with $D_{CO_2}=1.38\times10^{-5}$ m^2 s^{-1} (Zhang et al., 2014). The mean speed of a gas molecule is defined as:

$$\bar{v}_i=\left(\frac{8N_A\kappa T}{\pi MW_i}\right)^{\frac{1}{2}} \tag{S2}$$

where N_A is the Avagadro's number, κ is the Boltzmann constant and T is the temperature.

The value of K_e for the SAPHIR chamber is estimated based on Eq. (S3) (Krechmer et al., 2016):

$$K_e=0.004+\left(5.6\times10^{-3}\right)(V)^{0.74} \tag{S3}$$

In the irreversible partitioning case, the wall loss behavior is governed by the wall accommodation coefficient. $\alpha_{w,i}$ Zhang et al. (2015) observed a strong negative correlation between $\alpha_{w,i}$ and the saturation concentration C_i^*, and they formulated an empirical expression for $\alpha_{w,i}$ as a function of C_i^* based on the measurements:

$$log_{10}\left(\alpha_{w,i}\right)=-0.1919\times log_{10}\left(C_i^*\right)-6.32 \tag{S4}$$

Table S3: Estimated wall loss rates of different dimers

Formula	Volatility range [a]	Used for yield calculation?	k_w (s^{-1})	τ_w (s)	τ_{dil} (s)
$C_{10}H_{16}N_2O_8$	SVOC	No	1.59E-05	8.67E+04	7.2E+04
$C_{10}H_{16}N_2O_9$	SVOC	No	2.99E-05	4.62E+04	7.2E+04
$C_{10}H_{16}N_2O_{10}$	LVOC	Yes	4.57E-05	2.82E+04	7.2E+04
$C_{10}H_{16}N_2O_{11}$	LVOC	Yes	7.76E-05	1.31E+04	7.2E+04
$C_{10}H_{16}N_2O_{12}$	LVOC	Yes	1.12E-04	8.30E+03	7.2E+04
$C_{10}H_{16}N_2O_{13}$	ELVOC	Yes	2.02E-04	3.18E+03	7.2E+04
$C_{10}H_{17}N_3O_{12}$	LVOC	Yes	6.62E-05	3.63E+04	7.2E+04
$C_{10}H_{17}N_3O_{13}$	LVOC	Yes	1.33E-04	1.10E+04	7.2E+04
$C_{10}H_{17}N_3O_{14}$	ELVOC	Yes	1.87E-04	7.96E+03	7.2E+04
$C_{10}H_{17}N_3O_{15}$	ELVOC	Yes	3.61E-04	2.03E+03	7.2E+04
$C_{10}H_{17}N_3O_{16}$	ELVOC	Yes	5.25E-04	1.10E+03	7.2E+04

[a] estimated by the median value of C^* from different vapor pressure calculation methods used in this study

Table S4: Average carbon oxidation state ($\overline{OS_C}$) measured from ambient or different isoprene oxidation systems

	$\overline{OS_C}$	Technique	Ref.
Chamber measurements			
1. Gas-phase products			
Isoprene + NO$_3$	-0.35 to + 0.09	Br$^-$ CIMS	This study
Isoprene 4-hydroxy-3-hydroperoxy (4,3-ISOPOOH) + OH	avg. +0.10	NO$_3^-$ CIMS	Krechmer et al., 2015
2. Secondary organic aerosol			
Isoprene + OH	~ -1.3	AMS	Aiken et al., 2008
Isoprene + O$_3$	-0.31 (+)/ -0.25 (-) [a]	ESI-MS	Nguyen et al., 2010
Isoprene + OH	-0.53 to -0.35	AMS	Chhabra et al., 2010
4,3-ISOPOOH + OH	avg. +0.05	AMS	Krechmer et al., 2015
Isoprene + OH	avg. -0.7	AMS	Lambe et al., 2015
Isoprene + Cl	-0.5 to +1.8	ACSM	Wang and Ruiz, 2018
Ambient measurements			
1. Ambient organic aerosol			
Mexico City, US	-1.54 to +0.11	AMS	Aiken et al., 2008
Amazonia	-0.9 to -0.2	AMS	Chen et al., 2009
Whistler Peak, Canada	avg. -0.14	AMS	Sun et al., 2009
Kaiping, China	avg. -0.54	AMS	Huang et al., 2011
Melpitz, Germany	avg. -0.47(su)/ -0.4(a)/ -0.41(w) [b]	AMS	Poulain et al., (2011)
Hongkong, China	avg. -0.59 (sp)/ -0.32 (su)/ -0.55 (a)/ -0.54 (w) [b]	AMS	Li et al., 2015
Mount Wuzhi, China	avg. +0.64	AMS	Zhu et al., 2016
Lake Hongze, China	avg. -0.18	AMS	Zhu et al., 2016
Beijing, China	avg. -0.64 (sp)/ -0.54 (su)/ -0.66 (a)/ -0.58 (w) [b]	AMS	Hu et al., 2017
Houston, US	avg. -0.09	AMS	Al-Naiema et al., 2018
Seoul, Korea	avg. -0.80	AMS	Kim et al., 2018
Zurich, Switzerland	avg. -0.31 (w)/ -0.25 (su) [b]	ESI-UHR-MS	Daellenbach et al., 2019
Hyytiälä, Finland	avg. -0.66 (2011)/ -0.36 (2014) [c]	ESI-UHR-MS	Daellenbach et al., 2019
Waliguan, China	avg. +0.55	AMS	Zhang et al., 2019
Yorkville, US	avg. +0.15	FIGAERO-CIMS	Chen et al., 2020
Yorkville, US	avg. -0.12	AMS	Chen et al., 2020
Xinglong, China	avg. -0.01 (sp)/ + 0.10 (su)/ 0.26 (a)/ -0.45 (w) [b]	AMS	Li et al., 2021

Oklahoma, US	avg. +0.289 (sp)/ -0.34 (su) [b]	AMS	Liu et al., 2021
2. **Ambient aerosol fractions**			
Hydrocarbon-like OA (HOA)	-1.7 to -1.6	AMS	Aiken et al., 2008
Oxygenated OA type I (OOA-I)	-0.5 to 0.0	AMS	Aiken et al., 2008
Oxygenated OA type II (OOA-II)	+ 0.5 to +0.9	AMS	Aiken et al., 2008
Daytime more oxidized OA	avg. +0.50	FIGAERO-CIMS	Chen et al., 2020
Daytime ON-rich OA	avg. +0.35	FIGAERO-CIMS	Chen et al., 2020
Morning less oxidized OA	avg. -0.13	FIGAERO-CIMS	Chen et al., 2020
Afternoon less oxidized OA	avg. +0.04	FIGAERO-CIMS	Chen et al., 2020
Nighttime ON-rich OA	avg. +0.13	FIGAERO-CIMS	Chen et al., 2020
OOA-I	avg. +0.14 (sp)/ -0.099 (su) [b]	AMS	Liu et al., 2021
OOA-II	avg. -0.315 (sp)/ -0.264 (su) [b]	AMS	Liu et al., 2021
Isoprene-epoxydiol-derived SOA (IEPOX SOA)	avg. +1.606 (sp)/ -0.096 (su) [b]	AMS	Liu et al., 2021
HOA	avg. -1.91	AMS	Al-Naiema et al., 2018
Cooking-influenced less-oxidized oxygenated OA	avg. -0.35	AMS	Al-Naiema et al., 2018
More-oxidized oxygenated OA	avg. +1.27	AMS	Al-Naiema et al., 2018
3. **Gas-phase products**			
Centreville, US	avg. -0.043	NO_3^- CIMS	Massoli et al., 2018

[a] Values calculated separately for data from the positive (+) and negative (-) ion mode mass spectra

[b] Values calculated separately for data collected in spring (sp), summer (su), autumn (a) and winter (w).

[c] Values calculated for data collected in 2011 and 2014
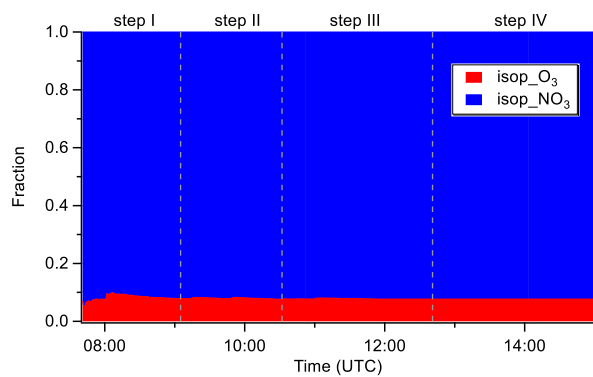
Figure S1: Fraction of isoprene consumed by O_3 and NO_3 calculated from measurements. The amount of isoprene consumed by O_3 was calculated from the measured concentrations of O_3 and isoprene, and that consumed by NO_3 was calculated from total isoprene losses (from isoprene measurements) subtracting losses due to dilution and reaction with O_3. Isoprene losses due to reaction with OH could not be included here, because the OH concentration was below the detection limit. However, according to model calculations OH contributed about 100% to the isoprene consumption (Vereecken et al., 2021).

13
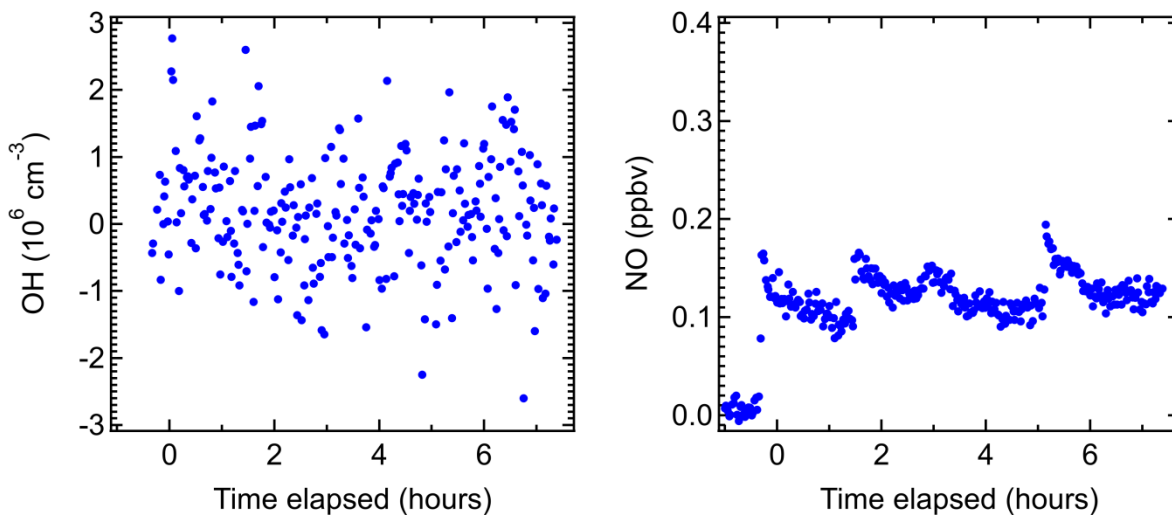
Figure S2: Concentrations of OH radical and NO during the isoprene-NO₃ experiment on 08 August, 2018. The OH concentration was measured by a laser-induced fluorescence (LIF) spectroscopy, and the NO mixing ratio was detected by a chemiluminescence analyzer. It should be pointed out that there was no NO in the chamber under dark condition, because the lifetime of NO would be very short under high O₃ condition. The non-zero values of NO are measurement artefacts due to the relatively high NO₂ concentration.
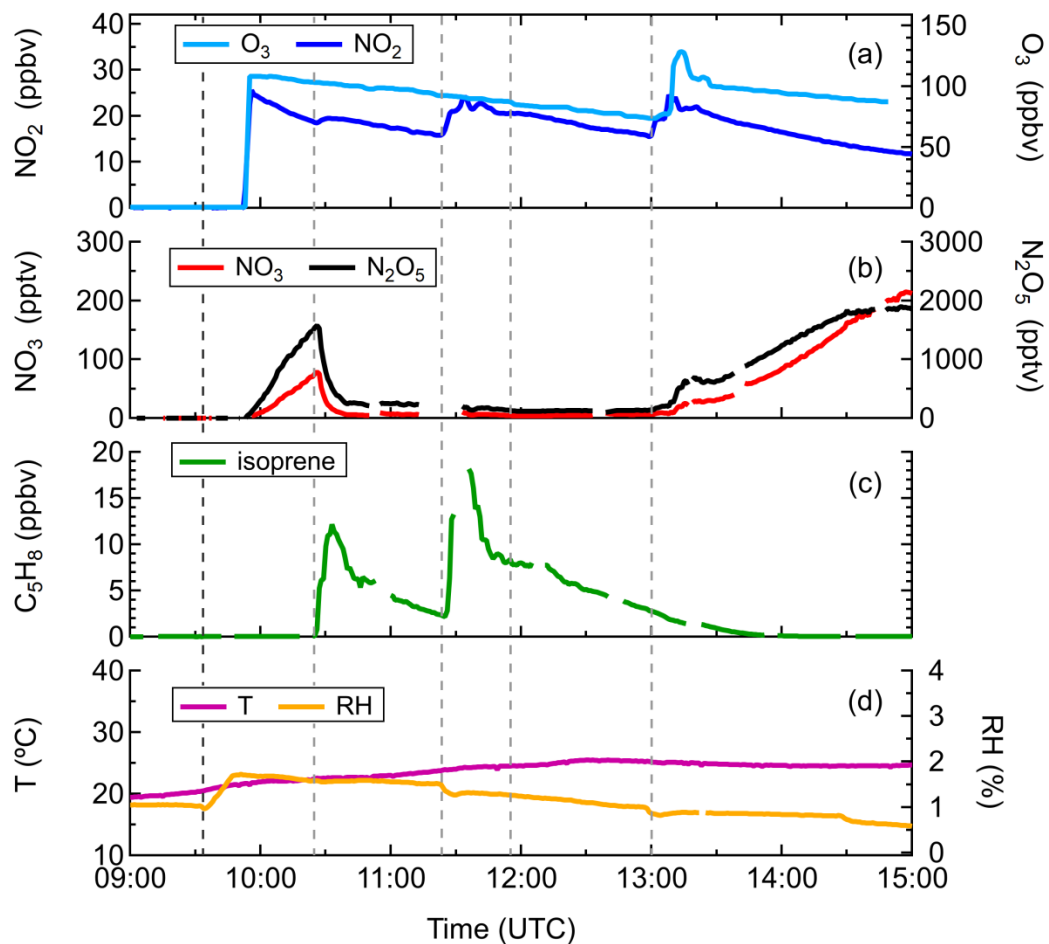
Figure S3: Measurements of (a) O₃ and NO₂, (b) NO₃ and N₂O₅, (c) isoprene and (d) temperature and relative humidity in the chamber during the experiment on 14 August, 2018.
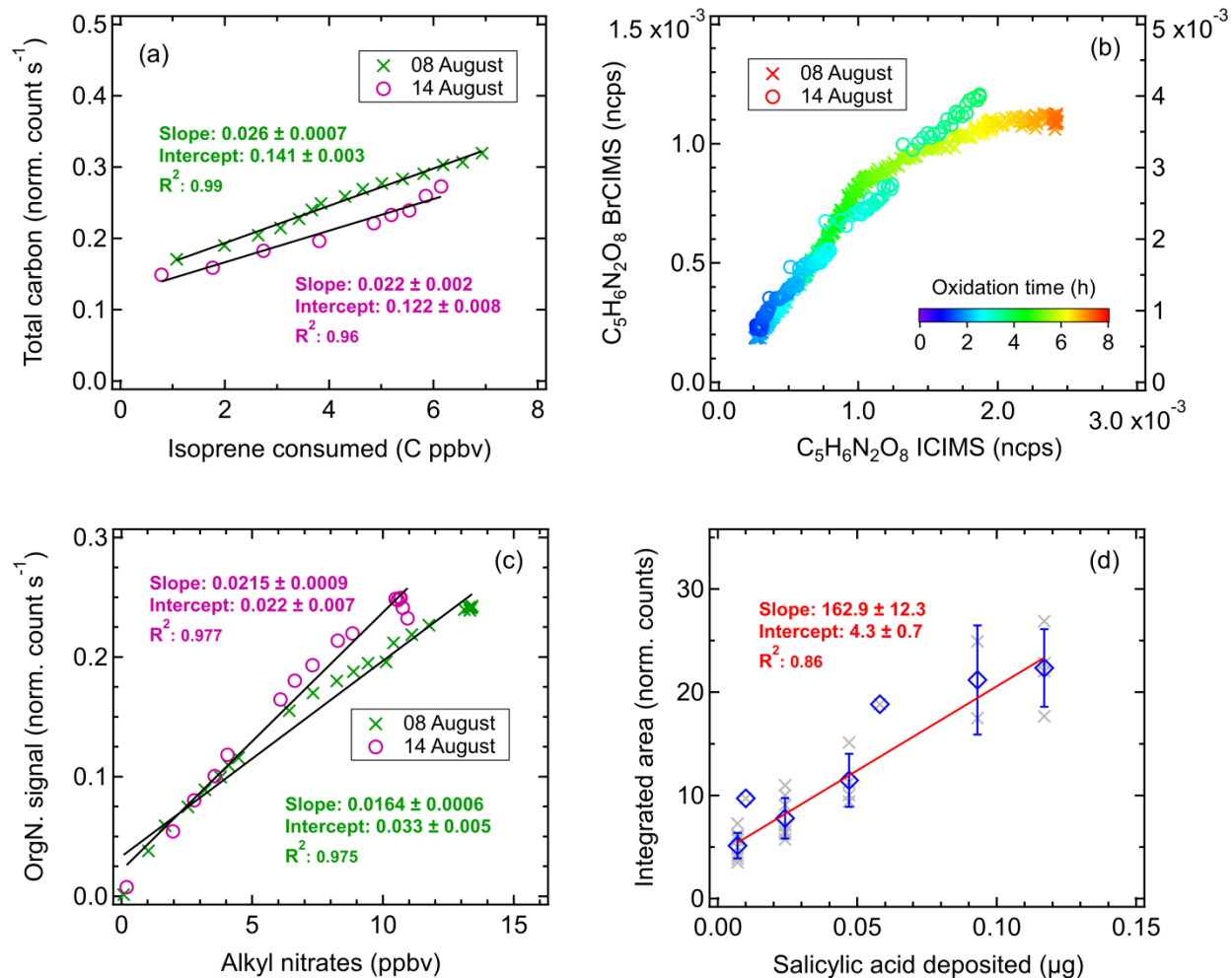
Figure S4: (a) Total carbon detected by Br⁻-CIMS versus isoprene consumed on 08 and 14 August, 2018. The sensitivity of CIMS for total carbon is determined by the slope of linear fit. The data have been corrected for dilution and wall losses. (b) Comparison of $C_5H_6N_2O_8$ measurements by Br⁻ CIMS and I⁻ CIMS. (c) Organonitrates measured by Br⁻ CIMS plotted against gas-phase alkyl nitrates measured by TDCRDS. The bulk sensitivity for organonitrates is determined by the slope of linear fit. (d) Calibration results of Br⁻ CIMS for salicylic acid.
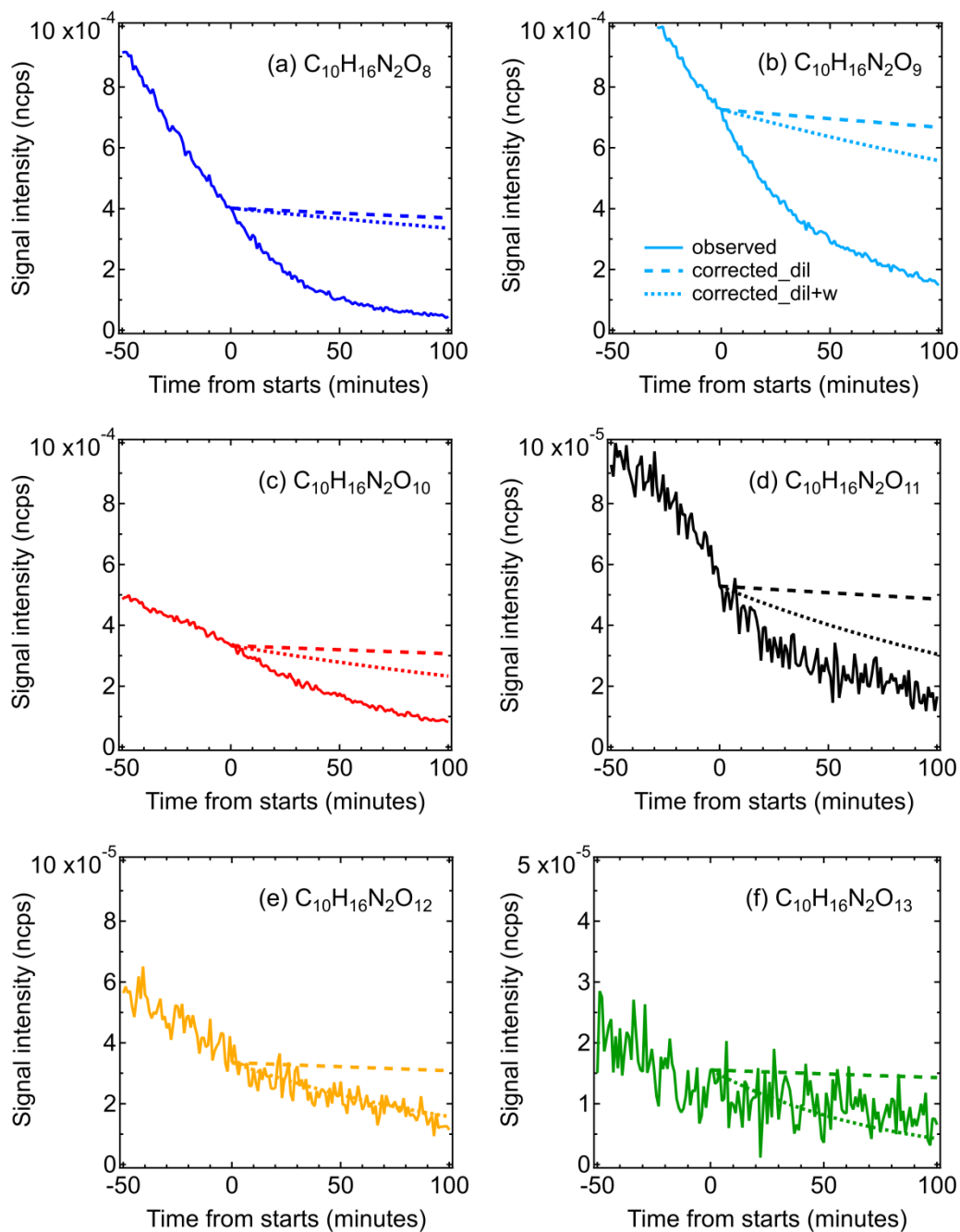
Figure S5: Comparison of the observed and predicted time evolution of 2N-dimers in step IV (only dilution or dilution and wall losses was considered). The time when the last injection of O₃ and NO₂ (without isoprene) occurred is set as zero.

17
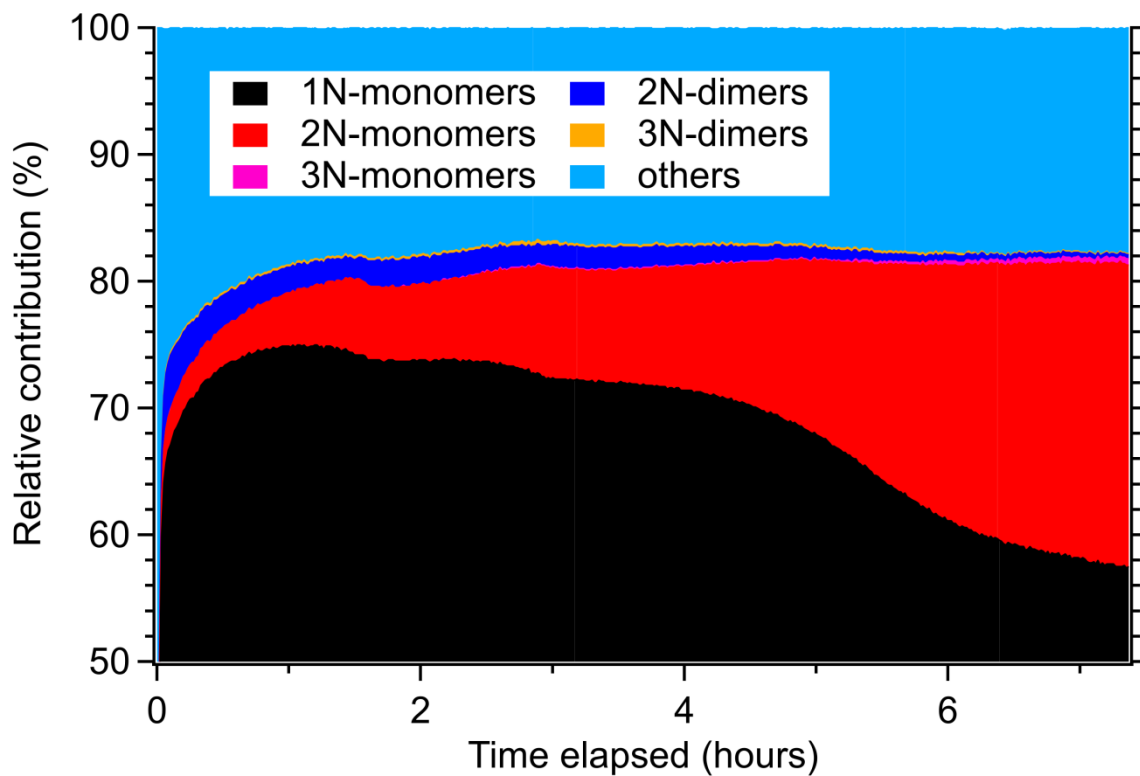
Figure S6: Time evolution of the relative contributions of different chemical groups measured by Br⁻-CIMS (only organic ions were counted for analysis). 'Others' refers to CHO compounds without containing nitrogen atoms (e.g., $C_5H_8O_2$ and $C_5H_8O_3$).
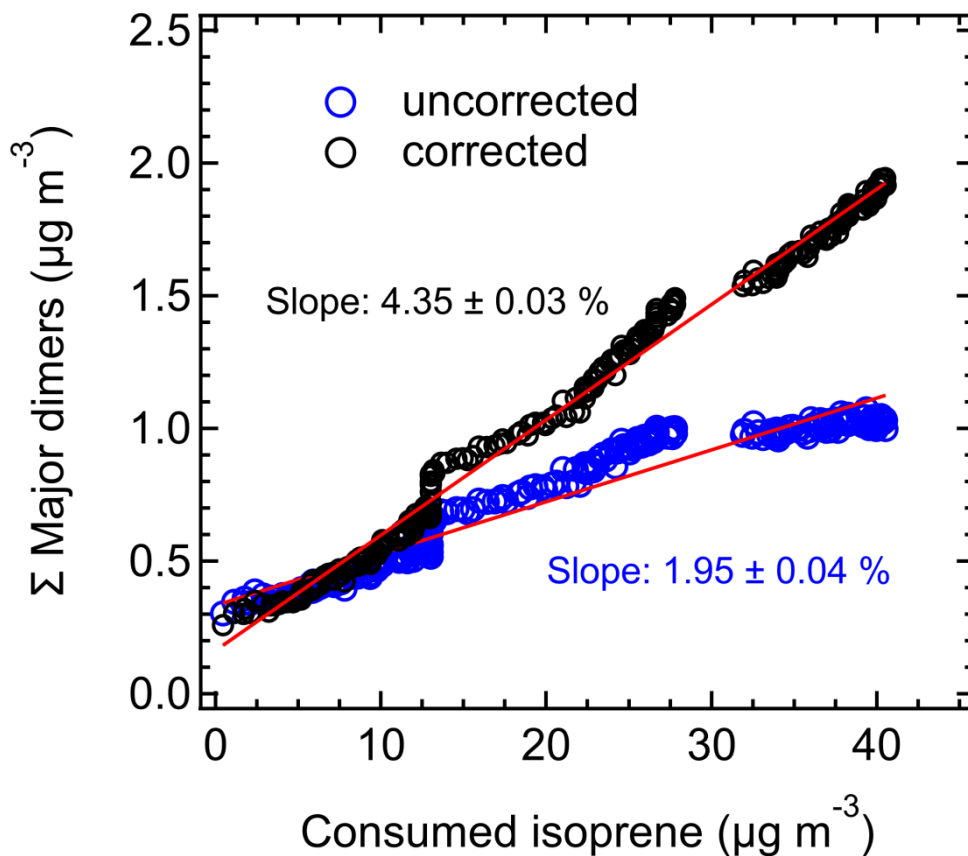
Figure S7: Major dimers mass as a function of consumed isoprene. Fitting a straight line to the data yields slopes of 1.95 ± 0.04 % and 4.35 ± 0.03 % for the uncorrected data and wall and dilution corrected data, respectively. The errors are the statistical errors of the fits. Wall loss corrections are shown in Table S3. Assuming all the dimers in the LVOC and ELVOC range can condense onto particles, producing SOA, we estimate a mass yield of about 5% ± 1.6 %. The relative uncertainty of SOA yield here was estimated to be 32% by using error propagation, which includes the uncertainty of the isoprene consumption concentration (~ 10%), the uncertainty of the alkyl nitrate concentration (~ 10%), the uncertainty of dimer content (~ 20%), and the uncertainty of estimated instrument sensitivity for organonitrates (~ 22%).
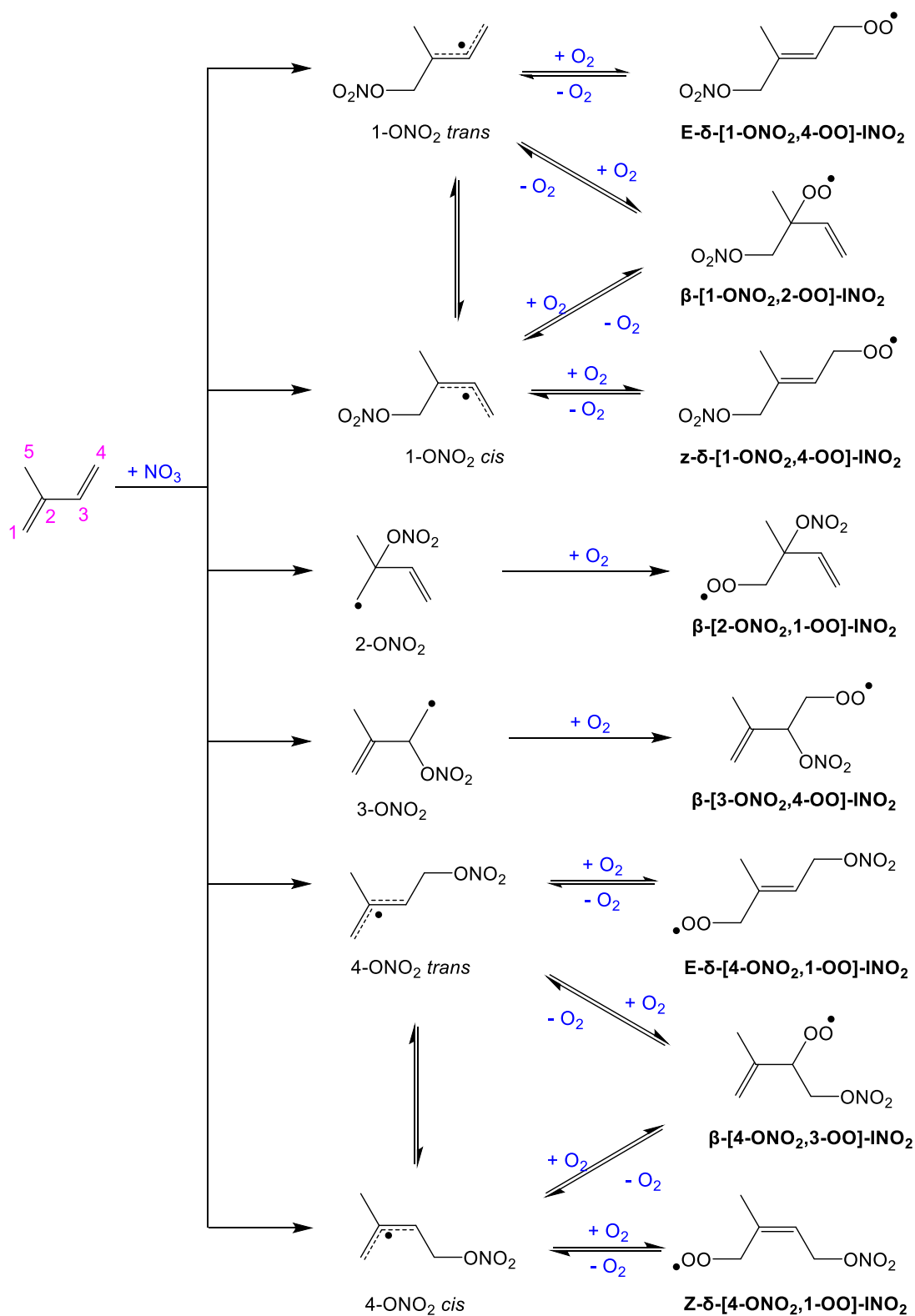
Scheme S1: Formation of isoprene nitrooxy peroxy radicals (INO₂) from NO₃-initiated oxidation with subsequent O₂ addition.

Scheme S2 – S4 serve to show which formula species can be expected in principle accoridng to the understanding of peroxy and alkoxy chemistry under consideration of intramolecular H-shifts and autoxoidation processes.
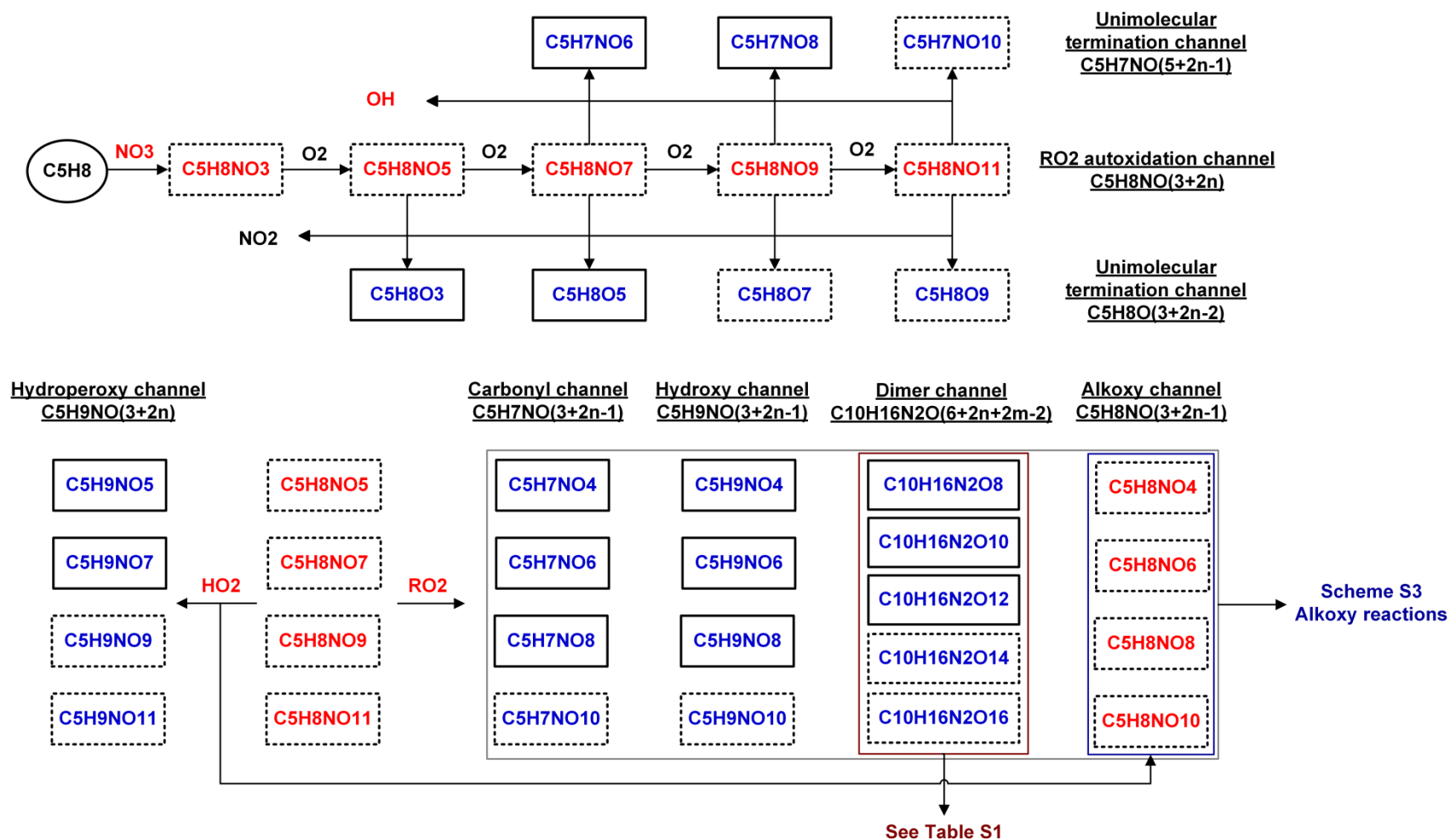
Scheme S2. Proposed first-generation reaction pathways of isoprene-NO₃ and the corresponding products. (n ≥ 1, number of autoxidation steps). Closed-shell products are presented in blue, while radicals are presented in red. Compounds with the given molecular formula in solid boxes have been detected by Br⁻ CIMS during the experiments, while those in dashed boxes have not.

21
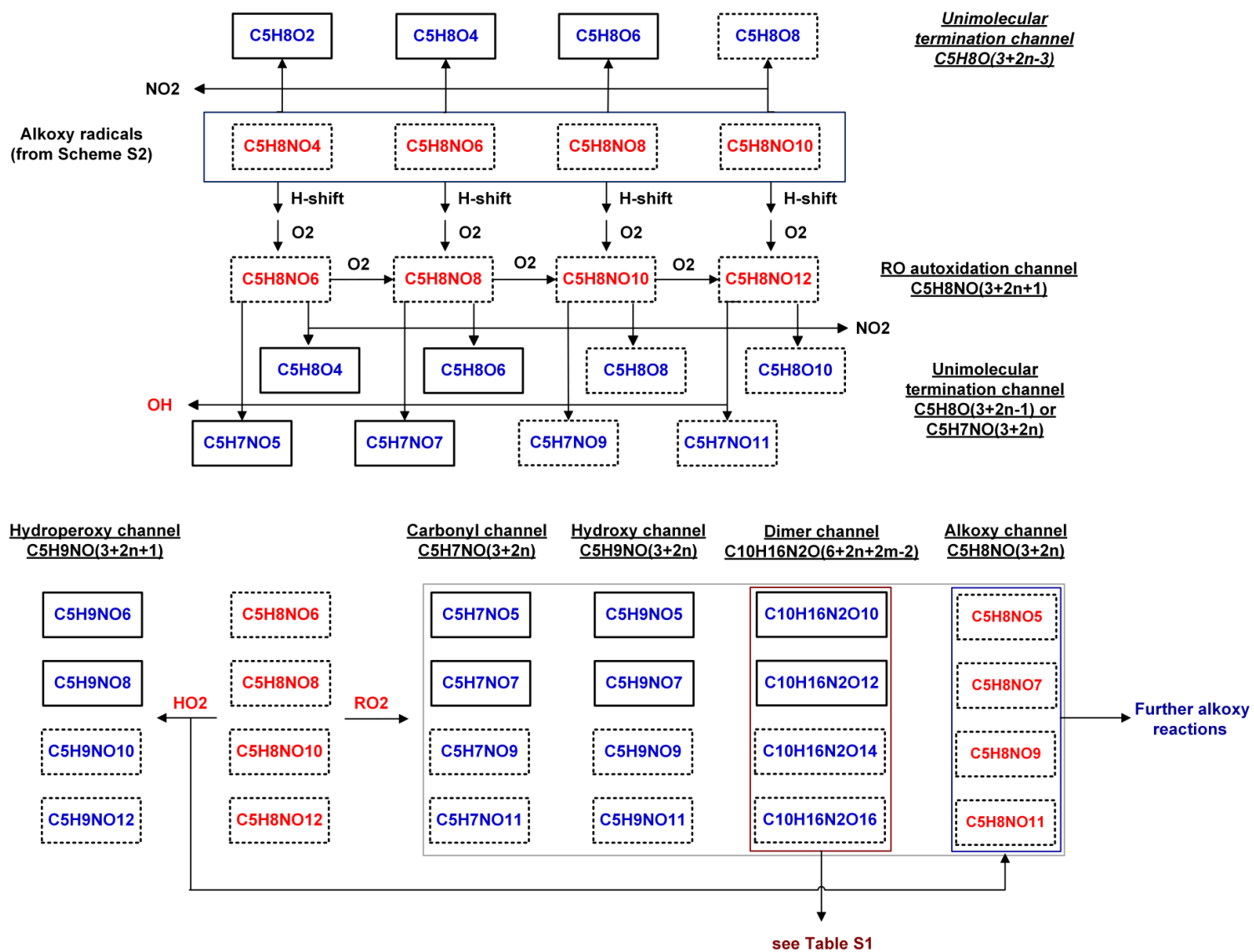
Scheme S3: Proposed reaction pathways of alkoxy radicals (formed from RO$_2$ alkoxy channel) and the corresponding products (n ≥ 1, number of autoxidation steps). Closed-shell products are presented in blue, while radicals are presented in red. Compounds with the given molecular formula in solid boxes have been detected by Br$^-$ CIMS during the experiments, while those in dashed boxes have not.

First-generation hydroxy and hydroperoxy products

C5H9NO4	C5H9NO6	C5H9NO8	C5H9NO10
C5H9NO5	C5H9NO7	C5H9NO9	C5H9NO11

H-shift H-shift H-shift H-shift

O2 O2 O2 O2

Unimolecular termination channel

NO2 +

C5H9NO7	C5H9NO9	C5H9NO11	C5H9NO13
C5H9NO8	C5H9NO10	C5H9NO12	C5H9NO14

C5H9N2O9 →O2→ C5H9N2O11 →O2→ C5H9N2O13 →O2→ C5H9N2O15

C5H9N2O10 →O2→ C5H9N2O12 →O2→ C5H9N2O14 →O2→ C5H9N2O16

Unimolecular termination channel

+ OH

C5H8N2O10	C5H8N2O12	C5H8N2O14
C5H8N2O9	C5H8N2O11	C5H8N2O13	C5H8N2O15

Hydroperoxy channel

C5H10N2O9	C5H10N2O10
C5H10N2O11	C5H10N2O12
C5H10N2O13	C5H10N2O14
C5H10N2O15	C5H10N2O16

HO2

C5H9N2O9	C5H9N2O10
C5H9N2O11	C5H9N2O12
C5H9N2O13	C5H9N2O14
C5H9N2O15	C5H9N2O16

RO2

Carbonyl channel

C5H8N2O8	C5H8N2O9
C5H8N2O10	C5H8N2O11
C5H8N2O12	C5H8N2O13
C5H8N2O14	C5H8N2O15

Hydroxy channel

C5H10N2O8	C5H10N2O9
C5H10N2O10	C5H10N2O11
C5H10N2O12	C5H10N2O13
C5H10N2O14	C5H10N2O15

Dimer channel

C10H17N3O12	C10H18N4O16
C10H17N3O13	C10H18N4O17
C10H17N3O14	C10H18N4O18
C10H17N3O15	C10H18N4O19

Alkoxy channel

C5H9N2O8	C5H9N2O9
C5H9N2O10	C5H9N2O11
C5H9N2O12	C5H9N2O13
C5H9N2O14	C5H9N2O15

Further alkoxy reactions

see Table S1

Scheme S4: Proposed second-generation reaction pathways of isoprene-NO₃ and the corresponding products. The subsequent reactions of alkoxy radicals formed in this process are similar to those shown in Scheme S4, therefore not treated further here. Closed-shell products are presented in blue, while radicals are presented in red. Compounds with the given molecular formula in solid boxes have been detected by Br⁻ CIMS during the experiments, while those in dashed boxes have not.
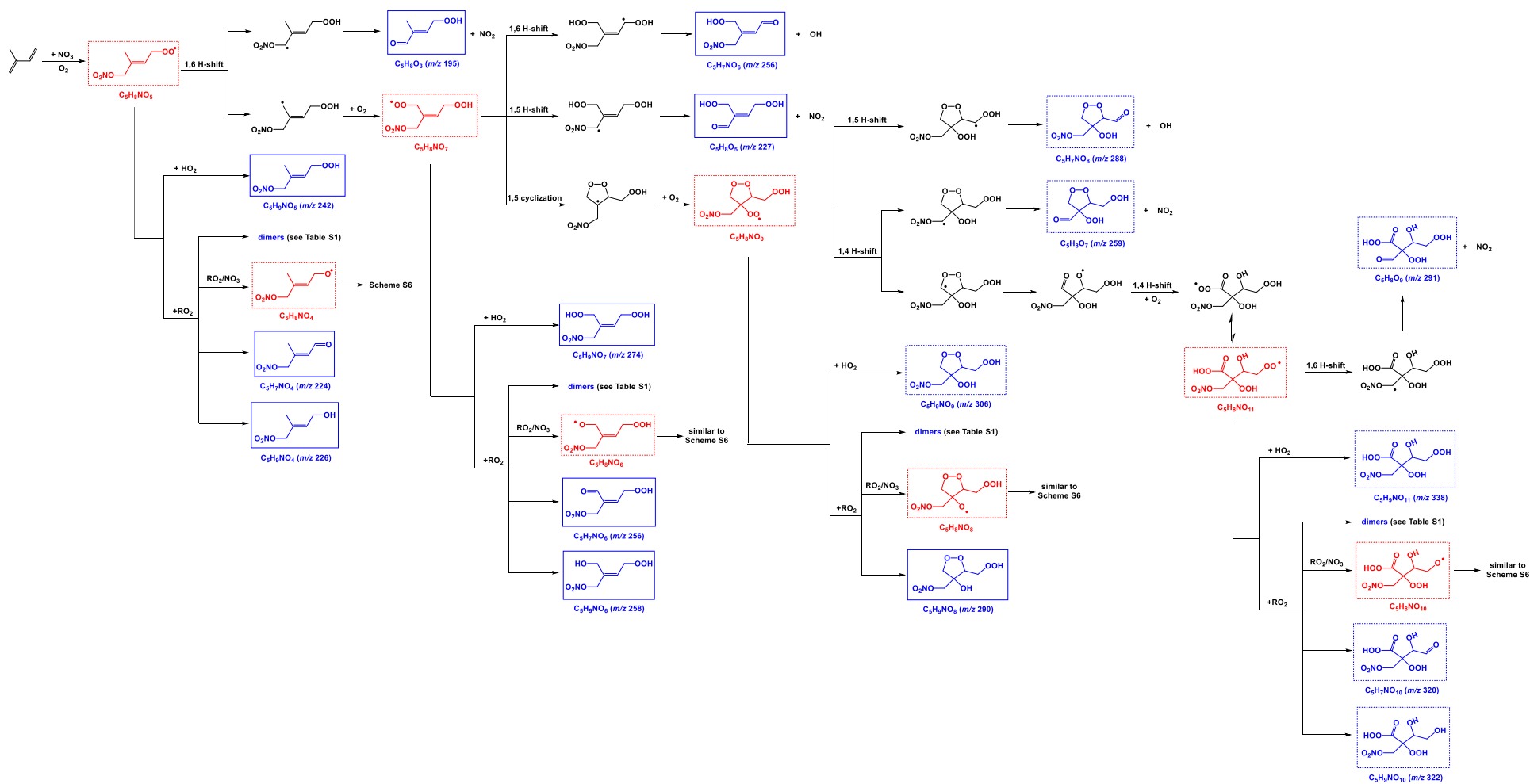
23

Scheme S5–S13 are exemplified realizations of reaction pathways shown in Scheme S2–S4 with the purpose to assess possible functionalities of compounds with the given molecular formula. They are used to calculate the range of vapor pressures covered by the observed formula compounds.

Scheme S5: General reactions and major gas-phase products formed following addition of NO₃ to isoprene. Only one situation is presented, so other isomers are possible. Compounds in blue are the major closed-shell products formed during the reaction, while those in red are major intermediates. Compounds with the given molecular formula in solid boxes have been detected by CIMS as Br⁻ adducts at the indicated *m/z* values, while those in dashed boxes have not.
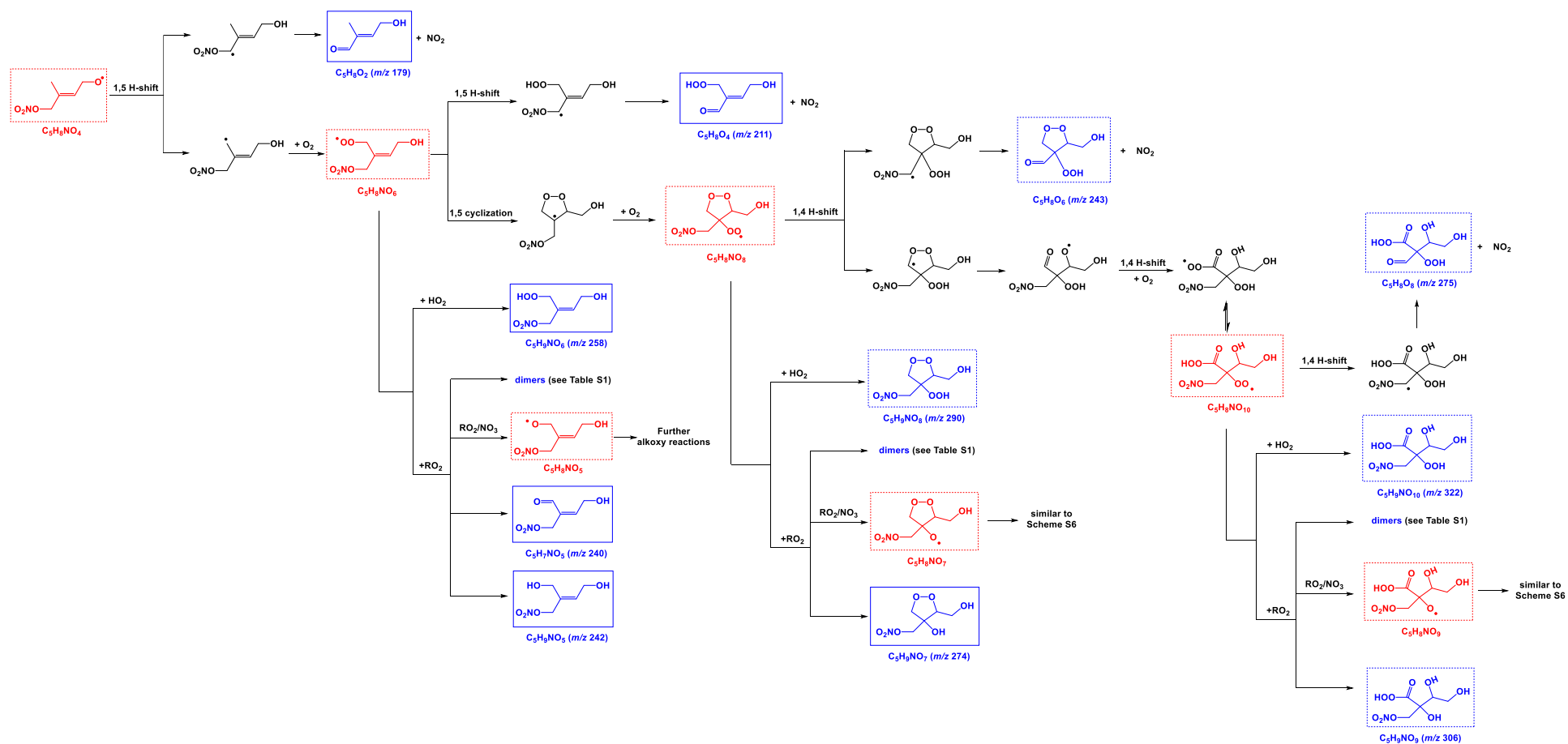
Scheme S6: General reactions and major products formed from rearrangement (H-shift) of the C_5 δ-[1,4]-nitrooxy alkoxy radical. Other isomers are possible. Compounds in blue are the major closed-shell products formed during the reaction, while those in red are major intermediates. Compounds with the given molecular formula in solid boxes have been detected by CIMS as Br⁻ adducts at the indicated *m/z* values, while those in dashed boxes have not.
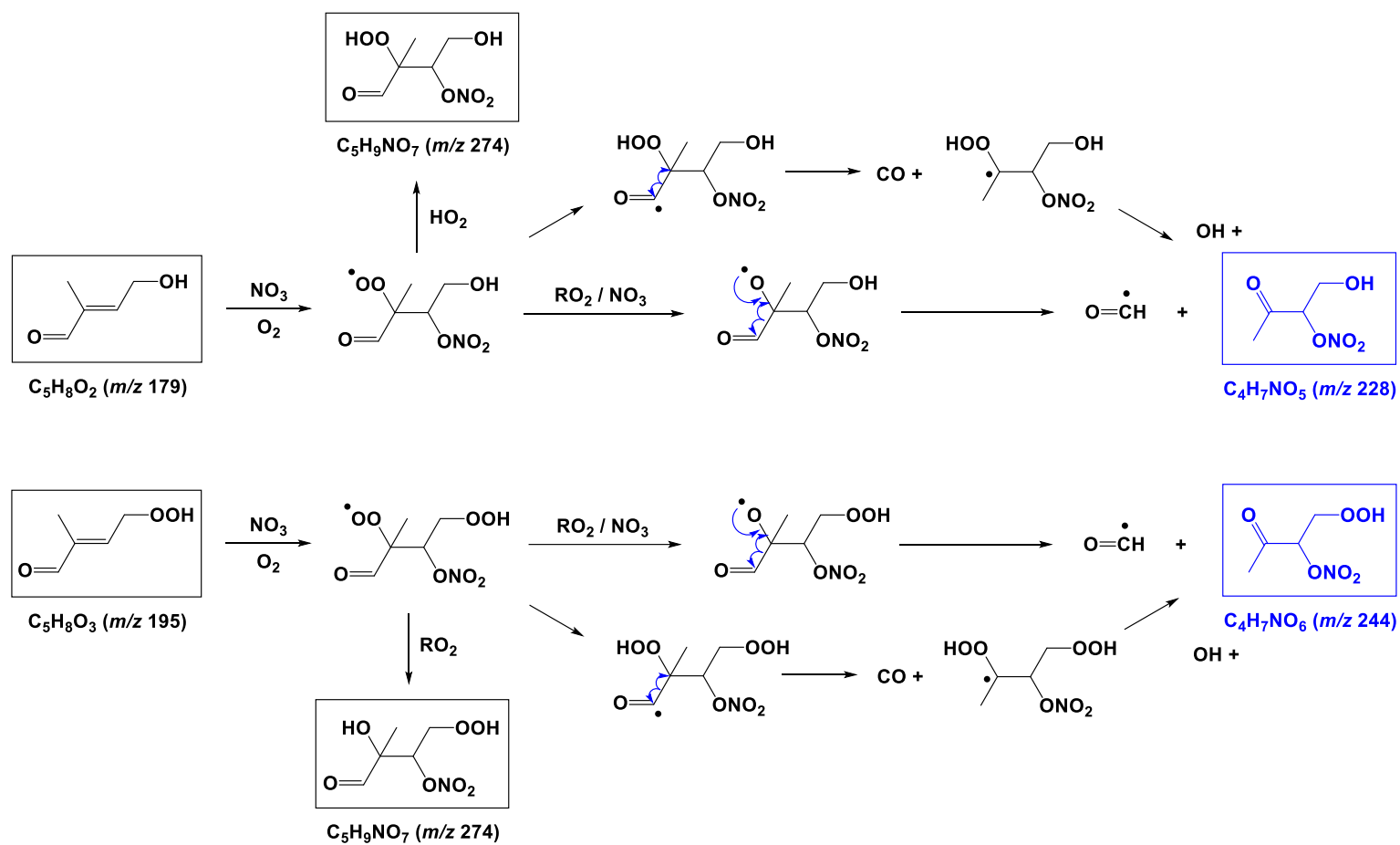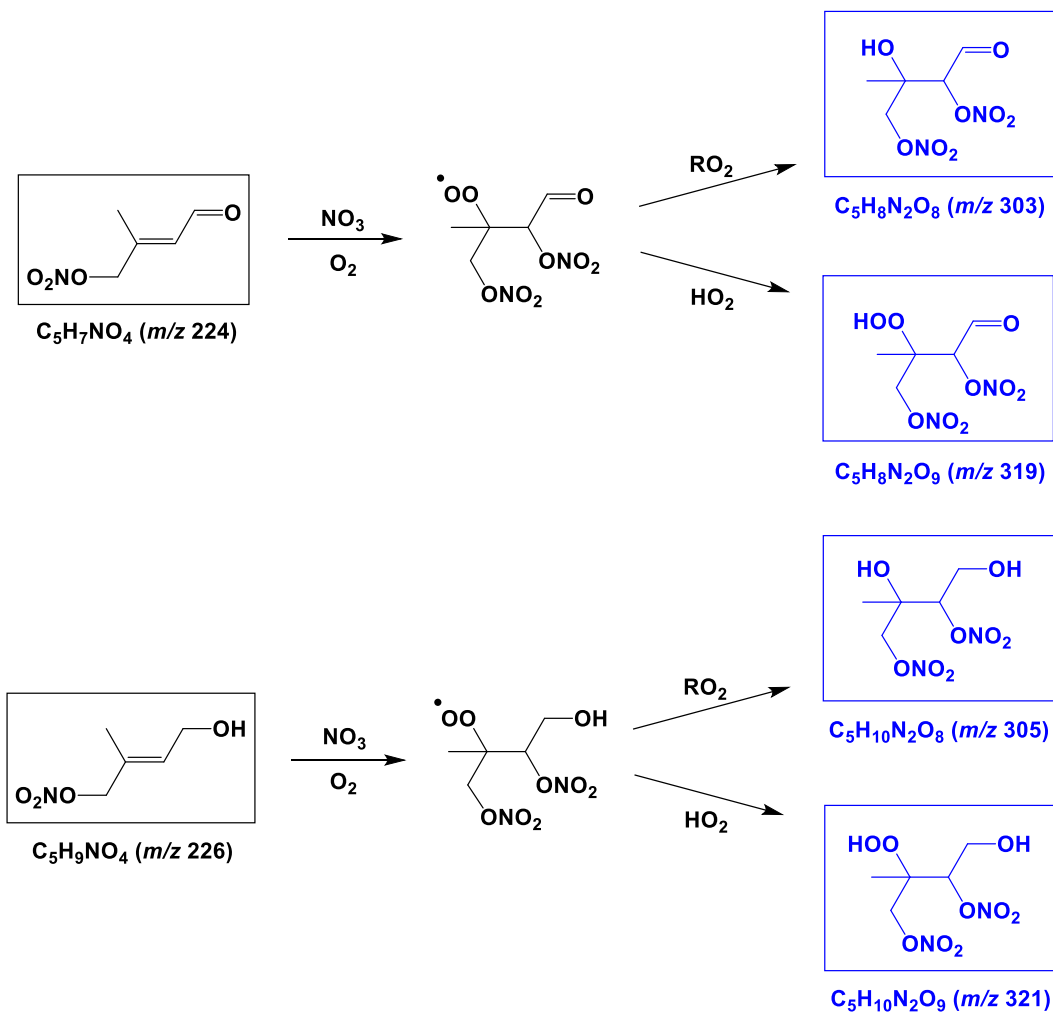
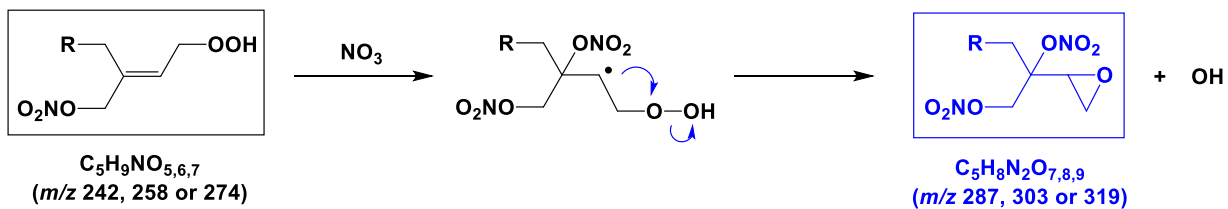**Scheme S7: Proposed formation mechanism of C₄ carbonyl nitrates (C₄H₇NO₅ and C₄H₇NO₆) from further oxidation of first-generation C₅ carbonyl products. Other isomers are possible. Compounds with the given molecular formula in boxes are closed-shell products detected by CIMS at the indicated *m/z* values.**

Scheme S8: Proposed formation mechanism of second-generation C$_5$ dinitrates. Here the major compounds C$_5$H$_{8,10}$N$_2$O$_{8,9}$ are taken as examples for illustration. Other isomers are possible. Compounds with the given molecular formula in boxes are closed-shell products detected by CIMS at the indicated m/z values.

R = H, OH or OOH

C₅H₉NO₅,₆,₇
(*m/z* 242, 258 or 274)

C₅H₈N₂O₇,₈,₉
(*m/z* 287, 303 or 319)

R' = OH or OOH

C₅H₈O₂,₃
(*m/z* 179 or 195)

C₅H₈N₂O₉,₁₀
(*m/z* 319 or 335)

Scheme S9: Proposed formation of dinitrooxy epoxides (upper panel) and petroxyacetyl nitrates (lower panel) from second-generation oxidation by NO₃ with subsequent rearrangement. Other isomers are possible. Compounds with the given molecular formula in boxes are closed-shell products detected by CIMS at the indicated m/z values.
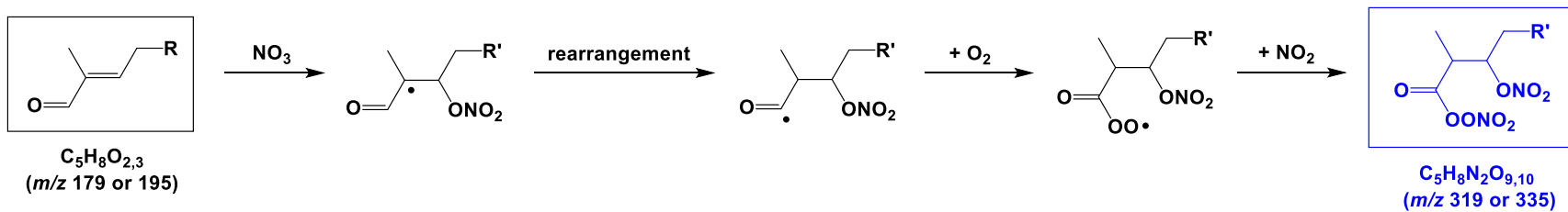
28

Scheme S10: Possible formation pathways of $C_5H_6N_2O_8$. Other isomers are possible. H-abstraction channel is adapted from MCM v3.3.1. Compounds with the given molecular formula in boxes are closed-shell products detected by CIMS at the indicated m/z values.
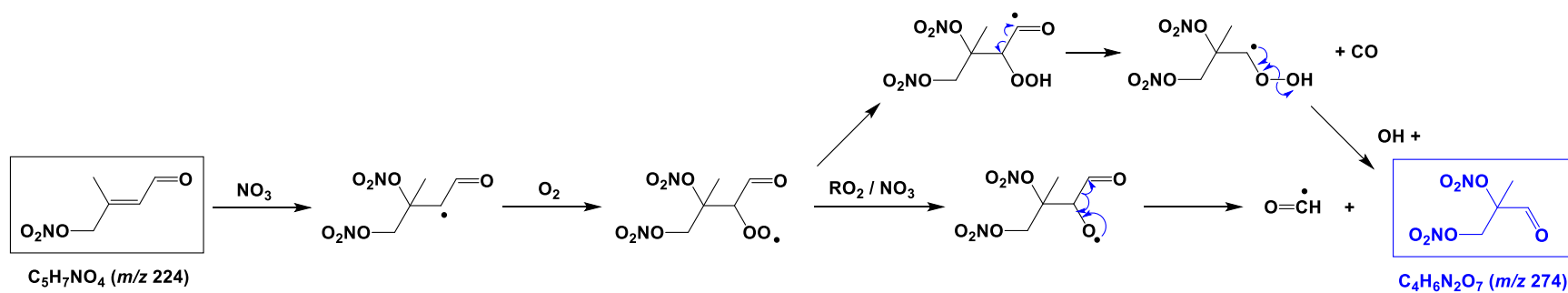
Scheme S11: Possible formation pathways of C₄H₆N₂O₇. Other isomers are possible. Compounds with the given molecular formula in boxes are closed-shell products detected by CIMS at the indicated m/z values.
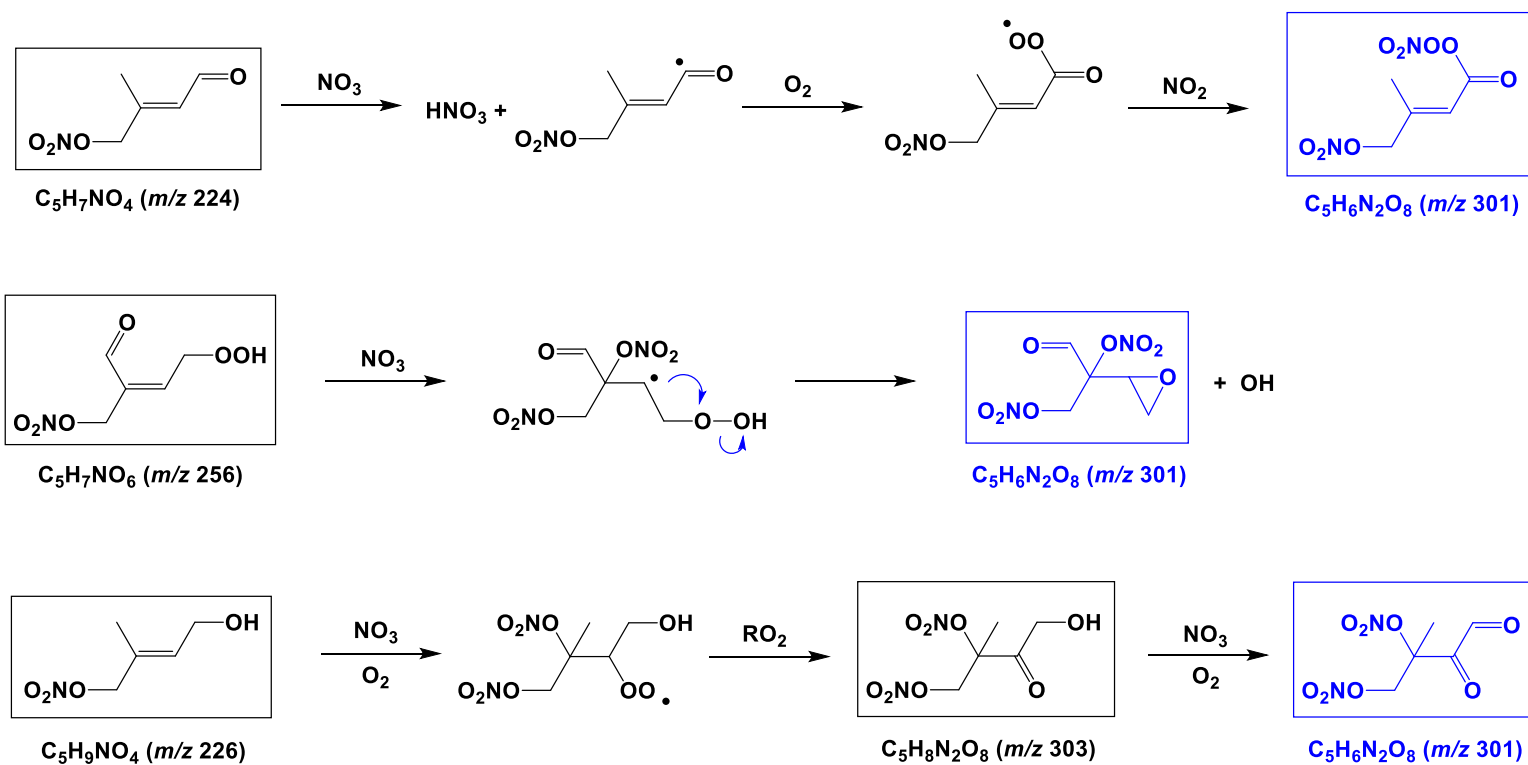
R_1 = H, OH
R_2 = OH, OOH

$C_5H_9NO_{4,5,6}$
(*m/z* 226, 242, or 258)

$C_5H_9N_3O_{10,11,12}$
(*m/z* 350, 366, or 382)
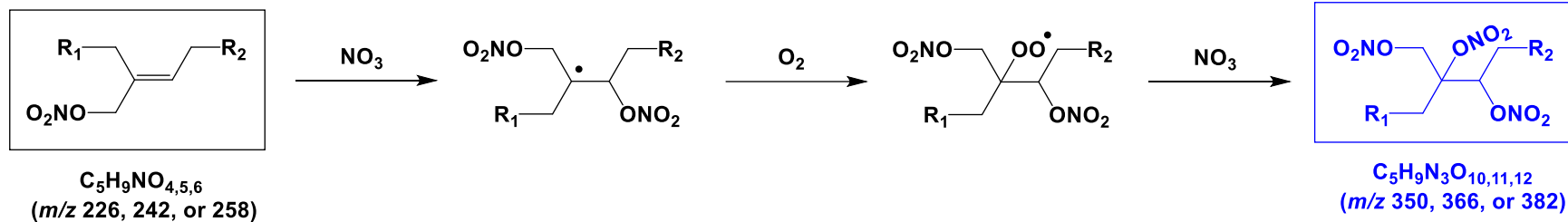
Scheme S12: Formation of trinitrates through further oxidation of the first-generation products by NO₃. Other isomers are possible. Compounds with the given molecular formula in boxes are closed-shell products detected by CIMS at the indicated m/z values.

31

Scheme S13: Proposed formation schematic of different types of dimers (colored by type) through RO₂ + R'O₂ reaction or further oxidation. Other isomers are possible. Compounds with the given molecular formula in boxes are closed-shell products detected by CIMS at the indicated m/z values.

References

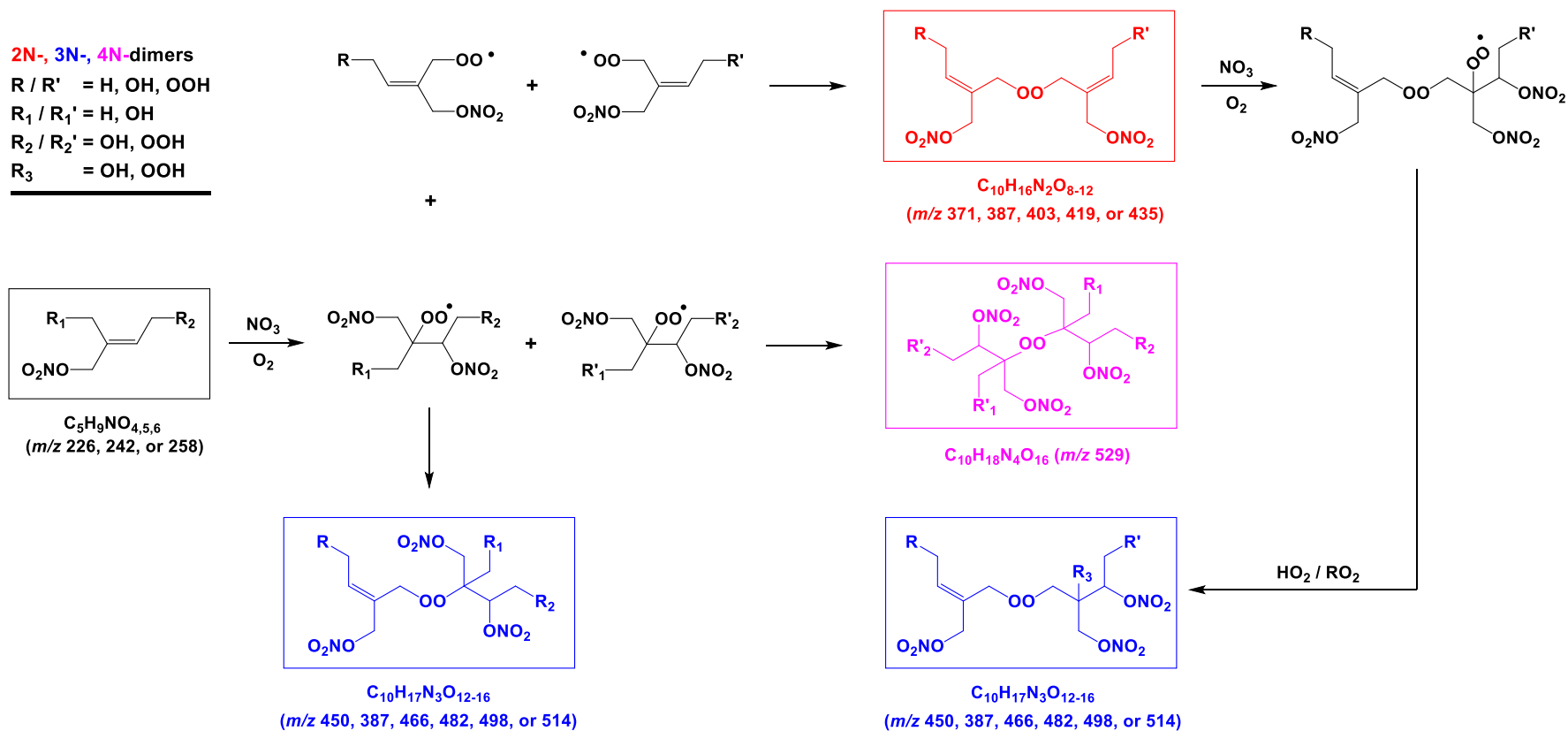Aiken, A. C., Decarlo, P. F., Kroll, J. H., Worsnop, D. R., Huffman, J. A., Docherty, K. S., Ulbrich, I. M., Mohr, C., Kimmel, J. R., and Sueper, D.: O/C and OM/OC ratios of primary, secondary, and ambient organic aerosols with high-resolution time-of-flight aerosol mass spectrometry, Environ. Sci. Technol., 42, 4478-4485, 2008.

Al-Naiema, I. M., Hettiyadura, A. P., Wallace, H. W., Sanchez, N. P., Madler, C. J., Cevik, B. K., Bui, A. A., Kettler, J., Griffin, R. J., and Stone, E. A.: Source apportionment of fine particulate matter in Houston, Texas: insights to secondary organic aerosols, Atmos. Chem. Phys., 18, 15601-15622, 2018.

Chen, Q., Farmer, D., Schneider, J., Zorn, S., Heald, C., Karl, T., Guenther, A., Allan, J., Robinson, N., and Coe, H.: Mass spectral characterization of submicron biogenic organic particles in the Amazon Basin, Geophys. Res. Lett., 36, 2009.

Chen, Y., Takeuchi, M., Nah, T., Xu, L., Canagaratna, M. R., Stark, H., Baumann, K., Canonaco, F., Prévôt, A. S., and Huey, L. G.: Chemical characterization of secondary organic aerosol at a rural site in the southeastern US: insights from simultaneous high-resolution time-of-flight aerosol mass spectrometer (HR-ToF-AMS) and FIGAERO chemical ionization mass spectrometer (CIMS) measurements, Atmos. Chem. Phys., 20, 8421-8440, 2020.

Chhabra, P., Flagan, R., and Seinfeld, J.: Elemental analysis of chamber organic aerosol using an aerodyne high-resolution aerosol mass spectrometer, Atmos. Chem. Phys., 10, 4111-4131, 2010.

Daellenbach, K. R., Kourtchev, I., Vogel, A. L., Bruns, E. A., Jiang, J., Petäjä, T., Jaffrezo, J.-L., Aksoyoglu, S., Kalberer, M., and Baltensperger, U.: Impact of anthropogenic and biogenic sources on the seasonal variation in the molecular composition of urban organic aerosols: a field and laboratory study using ultra-high-resolution mass spectrometry, Atmos. Chem. Phys., 19, 5973-5991, 2019.

Hu, W., Hu, M., Hu, W.-W., Zheng, J., Chen, C., Wu, Y., and Guo, S.: Seasonal variations in high time-resolved chemical compositions, sources, and evolution of atmospheric submicron aerosols in the megacity Beijing, Atmos. Chem. Phys., 17, 9979-10000, 2017.

Huang, X.-F., He, L.-Y., Hu, M., Canagaratna, M., Kroll, J., Ng, N., Zhang, Y.-H., Lin, Y., Xue, L., and Sun, T.-L.: Characterization of submicron aerosols at a rural site in Pearl River Delta of China using an Aerodyne High-Resolution Aerosol Mass Spectrometer, Atmos. Chem. Phys., 11, 1865-1877, 2011.

Kim, H., Zhang, Q., and Heo, J.: Influence of intense secondary aerosol formation and long-range transport on aerosol chemistry and properties in the Seoul Metropolitan Area during spring time: results from KORUS-AQ, Atmos. Chem. Phys., 18, 7149-7168, 2018.

Krechmer, J. E., Coggon, M. M., Massoli, P., Nguyen, T. B., Crounse, J. D., Hu, W., Day, D. A., Tyndall, G. S., Henze, D. K., and Rivera-Rios, J. C.: Formation of low volatility organic compounds and secondary organic aerosol from isoprene hydroxyhydroperoxide low-NO oxidation, Environ. Sci. Technol., 49, 10330-10339, 2015.

Krechmer, J. E., Pagonis, D., Ziemann, P. J., and Jimenez, J. L.: Quantification of gas-wall partitioning in Teflon environmental chambers using rapid bursts of low-volatility oxidized species generated in situ, Environmental science & technology, 50, 5757-5765, 2016.

Lambe, A., Chhabra, P., Onasch, T., Brune, W., Hunter, J., Kroll, J., Cummings, M., Brogan, J., Parmar, Y., and Worsnop, D.: Effect of oxidant concentration, exposure time, and seed particles on secondary organic aerosol chemical composition and yield, Atmos. Chem. Phys., 15, 3063-3075, 2015.

Li, J., Cao, L., Gao, W., He, L., Yan, Y., He, Y., Pan, Y., Ji, D., Liu, Z., and Wang, Y.: Seasonal variations in the highly time-resolved aerosol composition, sources and chemical processes of background submicron particles in the North China Plain, Atmos. Chem. Phys., 21, 4521-4539, 2021.

Li, Y., Lee, B. P., Su, L., Fung, J. C. H., and Chan, C. K.: Seasonal characteristics of fine particulate matter (PM) based on high-resolution time-of-flight aerosol mass spectrometric (HR-ToF-AMS) measurements at the HKUST Supersite in Hong Kong, Atmos. Chem. Phys., 15, 37-53, 2015.

Liu, J., Alexander, L., Fast, J. D., Lindenmaier, R., and Shilling, J. E.: Aerosol characteristics at the Southern Great Plains site during the HI-SCALE campaign, Atmos. Chem. Phys., 21, 5101-5116, 2021.

Massoli, P., Stark, H., Canagaratna, M. R., Krechmer, J. E., Xu, L., Ng, N. L., Mauldin, R. L., Yan, C., Kimmel, J., Misztal, P. K., Jimenez, J. L., Jayne, J. T., and Worsnop, D. R.: Ambient Measurements of Highly Oxidized Gas-Phase Molecules during the Southern Oxidant and Aerosol Study (SOAS) 2013, ACS Earth Space Chem., 2, 653-672, 10.1021/acsearthspacechem.8b00028, 2018.

Nguyen, T. B., Bateman, A. P., Bones, D. L., Nizkorodov, S. A., Laskin, J., and Laskin, A.: High-resolution mass spectrometry analysis of secondary organic aerosol generated by ozonolysis of isoprene, Atmos. Environ., 44, 1032-1042, 2010.

Poulain, L., Spindler, G., Birmili, W., Plass-Dülmer, C., Wiedensohler, A., and Herrmann, H.: Seasonal and diurnal variations of particulate nitrate and organic matter at the IfT research station Melpitz, Atmos. Chem. Phys., 11, 12579-12599, 2011.

Sun, Y., Zhang, Q., Macdonald, A., Hayden, K., Li, S., Liggio, J., Liu, P., Anlauf, K., Leaitch, W., and Steffen, A.: Size-resolved aerosol chemistry on Whistler Mountain, Canada with a high-resolution aerosol mass spectrometer during INTEX-B, Atmos. Chem. Phys., 9, 3095-3111, 2009.

Vereecken, L., Carlsson, P., Novelli, A., Bernard, F., Brown, S., Cho, C., Crowley, J., Fuchs, H., Mellouki, W., and Reimer, D.: Theoretical and experimental study of peroxy and alkoxy radicals in the NO3-initiated oxidation of isoprene, Phys. Chem. Chem. Phys., 23, 5496-5515, 2021.

Wang, D. S., and Ruiz, L. H.: Secondary organic aerosol from chlorine-initiated oxidation of isoprene, Atmos. Chem. Phys., 17, 13491-13508, 2017.

Zhang, X., Cappa, C. D., Jathar, S. H., McVay, R. C., Ensberg, J. J., Kleeman, M. J., and Seinfeld, J. H.: Influence of vapor wall loss in laboratory chambers on yields of secondary organic aerosol, Proceedings of the National Academy of Sciences, 111, 5802-5807, 2014.

Zhang, X., Schwantes, R., McVay, R., Lignell, H., Coggon, M., Flagan, R., and Seinfeld, J.: Vapor wall deposition in Teflon chambers, Atmospheric Chemistry and Physics, 15, 4197-4214, 2015.

Zhang, X., Xu, J., Kang, S., Zhang, Q., and Sun, J.: Chemical characterization and sources of submicron aerosols in the northeastern Qinghai–Tibet Plateau: insights from high-resolution mass spectrometry, Atmos. Chem. Phys., 19, 7897-7911, 2019.

Zhu, Q., He, L.-Y., Huang, X.-F., Cao, L.-M., Gong, Z.-H., Wang, C., Zhuang, X., and Hu, M.: Atmospheric aerosol compositions and sources at two national background sites in northern and southern China, Atmos. Chem. Phys., 16, 10283-10297, 2016.